Check for updates

Covalently functionalized graphene oxide wrapped by silicon–nitrogen-containing molecules: preparation and simultaneous enhancement of the thermal stability, flame retardancy and mechanical properties of epoxy resin nanocomposites†

Yanlong Sui,[a] Lijie Qu, [ID] [a] Peihong Li,[a] Xueyan Dai,[a] Qiangsheng Fang,[a] Chunling Zhang [ID] *[a] and Ying Wang*[b]

A novel functionalized graphene oxide (FGO) wrapped with Si–N-containing flame retardant (FR-fGO) was successfully synthesized *via* a chemical modification process and applied to enhance the thermal stability, fire resistance, and mechanical properties of epoxy resin (EP). Herein, Fourier transform infrared spectroscopy, X-ray diffraction, scanning electron microscopy, and transmission electron microscopy were used to explore the structure and morphology of FR-fGO to overcome the fact that the FGO cannot strongly bond with the polymer matrix. With the incorporation of FR-fGO into EP, the thermal stability improved and the total heat release decreased compared with pure EP. Meanwhile, FR-fGO composites significantly reduced the amount of flammable and toxic volatiles. A possible flame-retardant mechanism of FR-fGO was deduced from a theoretical analysis of the chemical bond energy and the experimental results of thermal decomposition: namely, well-dispersed FR-fGO nanosheets constituted a physical barrier, with an Si–N-containing synergy system forming a highly graphitized residual char with an Si-containing cross-linked network. The enhancement in mechanical properties demonstrated that the composites had remarkable compatibility. This study provides a novel modification strategy to improve the dispersion and flame retardance of graphene.

1. Introduction

In the past few years, graphene, as a two-dimensional (2D) carbon nanomaterial, has stimulated considerable interest into 2D layered materials because of its outstanding physical properties, such as large specific surface area and excellent thermal conductivity.[1,2] Graphene and its derivatives have been paid considerable attention as potential flame-retardant additives for polymers, thereby providing a brand new way of improving the flame resistance of polymers without damaging their intrinsic performance and endowing polymers with excellent mechanical properties.[3,4] The main flame-retardation mechanism of graphene and its derivatives is attributed to their barrier effect, which slows down the volatilization of gas degradation pyrolytic products and promotes the formation of

a protective char layer that is similar to a network-state structure in preventing the exchange process of heat and degradation products.[5] However, the aggregation and strong forces between the graphene sheets result in poor compatibility with polymer matrices.[6] A common way to overcome this problem is to modify the graphene surface. Grafting polymeric molecules through covalent bonding can effectively reduce the polarity of graphene and improve its dispersion.[7] Graphene oxide (GO), as a derivative of graphene, has become a research hotspot because its surface has many O-containing groups, such as OH and epoxy groups, on its basal planes, which can allow active sites to perform covalent functionalization.[8]

Epoxy resin (EP) is an extensively used thermosetting resin that has been widely applied in various industrial fields, such as adhesives, coatings, electronic materials, and high-performance composites, because of its good mechanical properties, considerable chemical resistance, and high thermal stability.[9,10] However, common EP is highly flammable, thereby restricting its further application to some extent.[11] Therefore, improving the flame retardancy of EP is crucial. Traditionally, halogenated compounds have been widely used for improving the flame retardancy of EP. Unfortunately, halogenated compounds generate a large amount of corrosive and toxic

[a]School of Materials Science and Engineering, Jilin University, Changchun 130025, PR China. E-mail: clzhang@jlu.edu.cn

[b]State Key Laboratory of Rare Earth Resource Utilization, Changchun Institute of Applied Chemistry, Chinese Academy of Sciences, Changchun 130022, PR China. E-mail: ywang_2012@ciac.ac.cn

† Electronic supplementary information (ESI) available. See DOI: 10.1039/d0ra01866j

gases during combustion.[12] With the increase in ecological and environmental concerns, halogen flame-retardants are limited and have stimulated worldwide activity in the search for halogen-free flame retardants.[13]

Several halogen-free flame retardants, such as phosphorus flame retardants,[14] inorganic particles,[15] and layered double hydroxide,[16] have been developed. Si–N-containing flame retardants have been extensively used to provide polymers with excellent flame retardancy. On the one hand, Si can provide a nanoscale Si–O–Si intramolecular hybridization structure, which is thermally stable and prevents matrix decomposition.[17] On the other hand, N generation reduces O concentration, which further reduces the release of toxic gases and smoke during combustion.[18] Zhang *et al.*[19] constructed a cross-linked network based on cyanate ester (CE) and hybridized GO with Si and N. CE composites not only had higher thermal stability but also achieved outstanding flame retardancy, producing more residual chars with graphitization, than with pure CE resin. However, most studies only added functionalized graphene to the matrix without considering its compatibility with the matrix and explaining its dispersion.[20]

In the present study, a novel Si–N-based decorated GO was prepared through a chemical modification process from the perspective of compatibility. The functionalized GO (FGO) with many active groups can easily form covalent bonds with the EP matrix, which not only improved its dispersion and compatibility in the matrix but also increased the flame-retarding efficiency of FGO after a series of tests. Molecular simulation will also be used to understand FGO/EP composites and its flame-retardant mechanism further.

2. Experimental

2.1 Materials

EP (DGETA) was purchased from Guangzhou Sui Xin Chemical Industrial Co., Ltd. (Guangdong, China). 2-(3,4-Epoxycydohexyl) ethyl triethoxysilane (ETEO) was provided by Sinopharm Chemical Reagent Co., Ltd. (Shanghai, China). $KMnO_4$, $NaNO_3$, H_2O_2 (30% aq.), absolute ethanol, H_2SO_4 (98%), and HCl (36.5%) were supplied by Beijing Chemical Works (Beijing, China). Graphite powder and 4,4-diaminodiphenylmethane (DDM) were obtained from Aladdin Reagent Co., Ltd. (Shanghai, China). All chemicals used in this work were of analytical grade and used without further treatment.

2.2 I-GO synthesis

GO was prepared from natural graphite *via* the Hummers' method.[21] GO surface modification was achieved as follows: 1.50 g of GO was dispersed in 250 ml of absolute ethanol and 20 ml of deionized water in a 500 ml three-neck flask *via* sonication for 1 h. A total of 2.00 g of ETEO was dissolved in 30 ml of absolute ethanol and 10 ml of deionized water and then added into the GO solution with additional sonication for 10 min. The resulting suspension was stirred for an additional time of 24 h at 70 °C. The FGO was washed with absolute ethanol and

deionized water successively. Finally, the dark brown solid was filtered and dried overnight under vacuum by a freeze dryer.

2.3 FGO wrapped with Si–N-containing flame retardant (FR-fGO) synthesis

The preparation of FR-fGO was as follows. First, 0.1 g of I-GO was dispersed in 50 ml of absolute ethanol in a 250 ml three-neck flask *via* sonication for 0.5 h. Then, the resulting suspension was stirred for 24 h at 80 °C. Meanwhile, a solution with 40 ml of absolute ethanol and 0.16 g of DDM was added into the flask dropwise for approximately 1 h. Finally, the black mixture was filtered and dried overnight under vacuum *via* freeze drying.

2.4 Preparation of epoxy/FR-fGO nanocomposites

The epoxy-based nanocomposites that contain FR-fGO flame retardant were prepared using the following procedures. First, FR-fGO was ultrasonically dispersed in acetone solution for 30 min. Second, the mixture was added into the EP, placed in the three-neck bottle, and continuously stirred for 12 h to remove residual solvent. Third, the curing agent (25 wt% relative to EP) was added into the aforementioned system and further stirred for 10 min. Finally, the uniform EP/FR-fGO mixture was decanted into a PTFE mold and cured at programmed temperatures of 105 °C, 155 °C, and 199 °C for 2 h. The composites were marked *x*FR-fGO/EP, where *x* represents the FR-fGO weight content relative to EP. I-GO/EP composites, were prepared by following the same process. Fig. 1 shows the preparation of I-GO, FR-fGO, and EP composites.

2.5 Characterization

Fourier transform infrared (FTIR) spectroscopy (Bruker TENSOR27) was performed in transmission mode with KBR pellets. X-ray diffraction (XRD) (Bruker D8 ADVANCE) was performed using a diffractometer equipped with Cu Kα radiation (λ = 0.154 nm). X-ray photoelectron spectroscopy (XPS) (Thermo ESCALAB 250) was performed to characterize the elements of graphene and char. The excitation source was an Al Kα line at
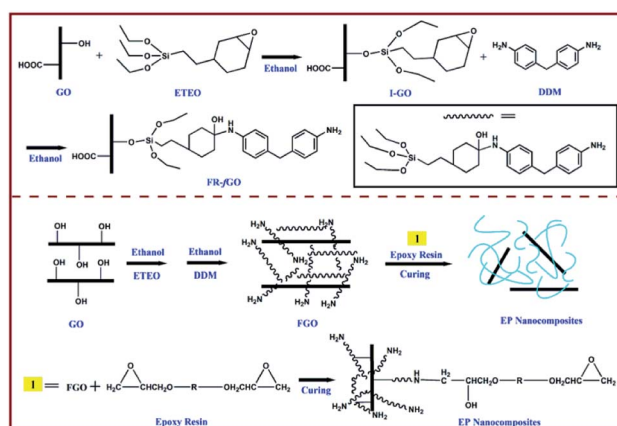

Fig. 1 Synthetic route of FR-fGO and curing process of FR-fGO/EP composites.

1486.6 eV. Thermogravimetric analysis (TGA) (PerkinElmer) was used under an N_2 atmosphere at a heating rate of 10 °C min^{-1} to investigate the pyrolysis behavior of the EP composites. Environment scanning electron microscopy (ESEM) (FEI XL-30), with an acceleration voltage of 10 kV, was utilized to observe the morphologies of GO and its derivatives, as well as the internal structure of the residual char from the cone test.

Energy dispersive X-ray (EDX) spectroscopy (OXFORD) that was connected to ESEM was used to investigate the elemental composition of the samples. Differential scanning calorimetry (DSC) (TA Q20) measured the glass transition behavior of the EP composites at a heating rate of 10 °C min^{-1} under nitrogen. Limiting oxygen index (LOI) values were measured using an LOI meter (FESTEC JF-3, Korea) with sheet dimensions of 80 mm × 6.5 mm × 3.2 mm, in accordance with ASTMD 2863-97. The UL-94 vertical burning properties of the EP composites were examined on a vertical burning tester (Motis Fire Technology UL94-X, China) with sheet dimensions of 125 mm × 12.7 mm × 3.2 mm, according to ASTMD 3801. A cone calorimetry test was performed using a calorimeter (iCone, FTT0242), in accordance with ISO 5660-1 standard, under a heat flux of 35 kW m^2 with a sample size of 100 mm × 100 mm × 5 mm. Py-GC/MS analysis was carried out by gas chromatography-mass spectrometry (GC/MS, Agilent 7890B, USA). The temperature of the GC/MS interface was 280 °C, and the cracker temperature was 500 °C. TGA-infrared spectrometry (TG-IR) was investigated using a TGA (iCone, 209F3) thermogravimetric analyzer that was linked to an FTIR (Brook, TENSOR27) spectrophotometer from 30 °C to 800 °C at 15 °C min^{-1} (N_2 atmosphere, flow rate of 30 ml min^{-1}). The degree of graphitization of samples was obtained using an inVia-Plus532 confocal Raman microprobe (Renishaw, UK). The detected wavenumber was between 800 cm^{-1} and 2000 cm^{-1}.

The mechanical properties of the EP composites were investigated using an electronic universal testing machine (WSM-5KN, China), in accordance with GBT 2567-2008.

2.6 Computation method

To explain the experimental phenomena, the stability of modified GO sheets was explored. Here, two characteristics were selected to describe the stability of the modified GO sheets: one was the energy gap (E_{gap}), and the other was the interactive energy of the chemical bonds. The geometries and energies were determined at the B3LYP/6-31++G(d, p) level of theory according to Gaussian 09 programs.[22] The simulation model of FR-fGO is shown in Fig. S1 in ESI.† The interaction energies of the C–N and Si–O bonds that existed in FR-fGO were also explored to explain the flame-retardant mechanism. The interaction energy of the molecule can be expressed with the following equation, according to a previous study:[23]

$$E_{int} = E_{XY} - E_X - E_Y, \tag{1}$$

where E_{XY} is the total energy of the FR-fGO molecule; E_X and E_Y are the energies of the two separated parts following C–N and Si–O bond breakage, respectively.

3. Results and discussion

3.1 Structure and morphology characterization of modified GO sheets

The FTIR spectra of GO, I-GO, and FR-fGO are presented in Fig. S2a.† The FTIR spectrum of GO exhibited the typical absorption peaks of O-containing groups. The peaks at approximately 3430 cm^{-1}, 1103 cm^{-1}, and 1726 cm^{-1} are attributed to the stretching vibrations of C–OH, C–O–C, and –COOH, respectively.[24] In the I-GO spectrum, the absorption bands in the region of 1000–1080 cm^{-1} were attributed to Si–O–C and Si–O–Si stretching vibrations and further proved successful chemical functionalization.[25] The FR-fGO was confirmed by the appearance of an absorption band at 1580 cm^{-1}, which is attributed to the –NH$_2$ bending vibration in FR-fGO; an absorption peak at 1290 cm^{-1} due to the C–N stretching vibration and a peak at 750 cm^{-1} corresponding to the C–H stretching vibration of the benzene ring,[26,27] indicating that the –NH$_2$ groups of DDM reacted with the active epoxy groups of I-GO. However, the N–H stretching vibration of FR-fGO at 3300 cm^{-1} could not be seen, possibly due to the overlap of the strong absorption of graphene sheets in this region. The FTIR results clearly indicated that amino group-rich FGO had been prepared successfully.

Fig. S2b† shows the XRD results of GO, I-GO, and FR-fGO. For GO, a sharp diffraction peak located at $2\theta = 10.9°$ corresponds to the (002) reflection. However, the diffraction peak disappeared after chemical modification, and the stacking structure of the GO sheets broke down and became disorderly, suggesting that the flame retardant was intercalated into the interlayer region of GO, further improving the flame-retardant efficiency. For I-GO, the weak peak at 23° may be due to the restacking of the exfoliated and modified GO sheets.[9] With further modification, the interlayer spacing of FR-fGO increased further, and no evident diffraction peaks appeared, suggesting that the flame retardant successfully wrapped the GO sheets.
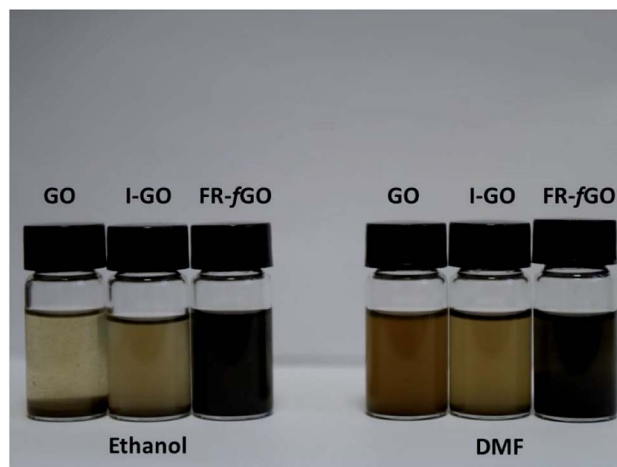

Fig. 2 Photographs of GO, I-GO, and FR-fGO dispersed in ethanol and DMF after standing for 6 h.

Fig. 2 shows the dispersity of GO, I-GO, and FR-fGO at a concentration of 1 mg ml^{-1} in two typical solvents (ethanol and DMF) after sonication (30 min). The figure shows that the GO aggregated in the upper layer in the two types of solvents after standing for 6 h. For I-GO, the digital image showed a significant precipitation in the solution. However, the precipitation rate had significantly reduced, which may be due to the fact that the modified ETEO reduced the polarity of I-GO. However, FR-fGO can readily form stable suspensions in ethanol and DMF because of the increase in defect structures after continuous modification, proving that GO was wrapped successfully.

XPS measurement was carried out to investigate the structure of GO sheets further and to confirm the simultaneous functionalization. The XPS survey scans of GO, I-GO, and FR-fGO (a) and the high-resolution C 1s XPS spectra of GO (b), I-GO (c), and FR-fGO (d) are shown in Fig. 3. The XPS spectrum of I-GO showed a significant increase in the Si 2s and Si 2p peaks compared with GO (Fig. 3a), which originated from ETEO. After adding DDM, N was observed in the XPS spectrum of FR-fGO, indicating that the flame retardant was completely grafted on the GO surface. To present further evidence of the successful preparation of FR-fGO, a high-resolution C 1s spectrum of GO is shown in Fig. 3b. This figure clearly shows that GO was fully oxidized, with four peaks appearing at C–C (284.5 eV), C–O (286.6 eV), C=O (287.4 eV), and C(O)OH (288.2 eV).[25] By contrast, the C 1s spectrum of I-GO (Fig. 3c) shows that the intensity of the O functional groups in I-GO decreased, indicating the removal of some O functional groups. However, a new peak at 285.4 eV, corresponding to the C–O–Si bond, appeared due to the hydrolysis between the alcoholic hydroxyl group and silanol.[28] In the C 1s spectrum of FR-fGO (Fig. 3d),

a significant increase in the intensity of the C–O–Si (286.6 eV) bond, which was due to a new C–N (286.5 eV) bond existing in DDM, appeared and overlapped with the C–O–Si bond and also caused the peak to move slightly to the left. These C–NH$_2$ groups would considerably improve the dispersion in the EP matrix, which would form strong interfacial interactions. The intensity of C–O group (286.6 eV) decreased, suggesting that the partial epoxy group had opened the ring and reacted with DDM. Besides, based on the XPS tests, the calculated contents of ETEO and DDM on the surface of FR-fGO were 13.9 and 8.5%, respectively. Thus, the ETEO and DDM that act as flame retardant are successfully wrapped on GO.

Fig. 4a–c show the SEM, EDX mapping images, and EDX spectrum of FR-fGO, respectively. The figures show that the surface became rough with a typical lamellar structure after modification (Fig. 4a). On the FR-fGO surface, C, O, Si, and N were detected after functionalization, and the elements were uniformly dispersed on the GO surface, illustrating the occurrence of the two-step reaction from GO to FR-fGO. The TEM images exhibited that GO showed a transparent and wrinkled morphology (Fig. 4d). For I-GO, a similar structure with a slightly darkened surface can be observed at the edge of the I-GO because of the Si being coated on the surface (Fig. 4e). After further modification (Fig. 4f), the thickness of FR-fGO increased compared with pristine GO and I-GO. The FR-fGO surface also became less transparent, and the dark features revealed that Si and N were successfully wrapped on the GO surface. The results also indicated that the modification of GO nanosheets changed the surface morphology. Thus, no evident aggregation was observed, which was beneficial to the uniform nanosheet distribution in the matrix.
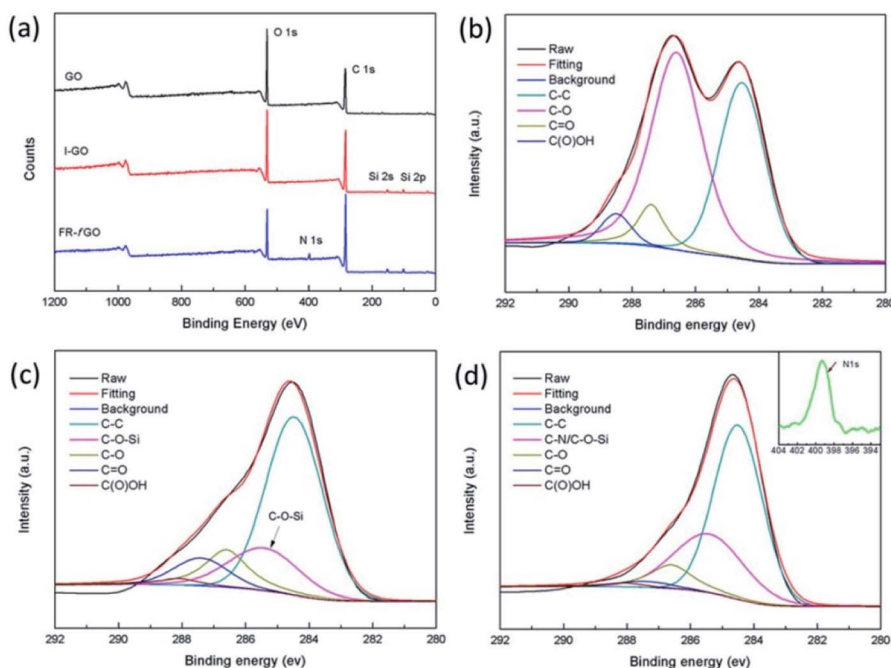

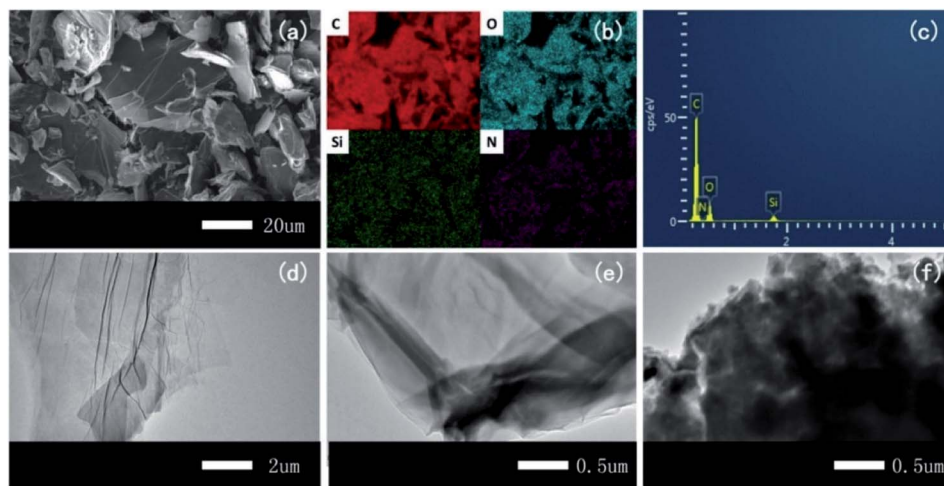Fig. 3   (a) XPS scans of GO, I-GO, and FR-fGO. C 1s spectra of (b) GO, (c) I-GO, and (d) FR-fGO.

Fig. 4 (a) SEM image of FR–fGO with (b) elemental mapping of C, O, Si, and N and (c) EDX results of FR–fGO. TEM patterns of (d) GO, (e) I-GO, and (f) FR–fGO.

3.2 Thermal properties of EP composites

DSC may provide information on the glass transition behavior of EP and its composites, which can explain the type of movement of molecular chains at different temperatures. Fig. S3† shows that the incorporation of GO or FR–fGO slightly influences the T_g of the EP composites. Pure EP exhibited a relatively low T_g value at 159.4 °C. With the incorporation of 0.5 wt% GO, the T_g of 0.5GO/EP increased by 0.9 °C. Meanwhile, the 0.5 wt% loading of FR–fGO in EP enhanced the T_g to 161.3 °C compared with that of GO. This phenomenon was due to the fact that multiactive amine groups on the surface of FR–fGO can react with the epoxy group in the EP matrix, thereby increasing the cross-link density. GO sheets also showed a steric hindrance that notably impeded the thermal movement of segments of the EP networks.[26] T_g is an indication of the relaxation behavior of the nanocomposite system. When the mobility of the polymer chains was constrained, thermal stability was improved. As the FR–fGO content increased, the cross-linked density gradually increased, and the confinement effect on the mobility of the polymeric network became strong. Thus, the T_g of the EP composites gradually increased. When 1.0FR–fGO was incorporated, the T_g value increased to 162.8 °C, with a 3.4 °C increase compared with that of pure EP.

Fig. S4† shows the TGA and DTG curves of GO and its functionalized products under a nitrogen atmosphere. The figure shows that the modified GO was the first to reach the maximum thermal decomposition rate. For FR–fGO, it was approximately 197.3 °C compared with I-GO (230 °C) and GO (226 °C). FR–fGO had the highest chemical activity. However, the GO and I-GO began to lose weight at <100 °C, and the maximum mass loss rate was significantly higher than that of FR–fGO because of the release of absorbed water and pyrolysis of the labile oxygen-containing functional groups.[29] The residual mass of FR–fGO was approximately 52.8%, whereas those of I-GO and GO were 51.2% and 40.5% at 800 °C, respectively. The thermal stability of FR–fGO was significantly improved relative to GO,

indicating that most of the O groups in GO were removed after functionalization, and the carbon skeleton was protected by Si–N-containing flame retardant. To investigate their chemical activity, we calculated the E_{gap} between the highest (HOMO) and lowest unoccupied molecular orbitals (LUMO) for GO, I-GO, and FR–fGO (Fig. S5†). The lower the E_{gap}, the easier it is for electrons to transfer from HOMO to LUMO,[30] suggesting a high chemical activity. FR–fGO had the smallest E_{gap} among the samples. Therefore, FR–fGO has the lowest kinetic stability and highest chemical activity, and can easily chemically bond to the substrate. These observations were in good agreement with our experiments.

Fig. S6† and Table 1 show the TG and DTG results of EP composites in an N_2 atmosphere, respectively. Here, all tested materials showed similar one-stage degradation behavior at 300 °C to 450 °C, which can be attributed to the thermal decomposition of the epoxy chain network. In Fig. S6a† the $T_{5 wt\%}$ of the EP composites was higher than the corresponding value of pure EP, which suggested that the addition of GO and FR–fGO delayed the initial decomposition temperature and increased the thermal stability of the composites. Meanwhile, when a small amount of GO and FR–fGO was incorporated, the $T_{50 wt\%}$ shifted to a low temperature, which was caused by the early degradation of the functional groups in GO and FR–fGO at low temperature. However, the 1.0FR–fGO/EP composite showed the highest $T_{50 wt\%}$, indicating that the introduction of FR–fGO formed a cross-linked network with the epoxy matrix and improved the thermal stability. The enhancement in residual char formation should be considered. At 700 °C, approximately 13.9% char residue was observed for pure EP. With the addition of 0.5 wt% GO and 0.5 wt% FR–fGO, 15.2% and 15.7% char residues became significantly higher than those of pure EP. This improvement was attributed to two factors. First, the GO sheets acted as physical barriers to protect the EP matrix from thermal degradation, and the flame-retardant molecular chains have a catalytic effect in char formation. Second, the flame retardant had good compatibility with the EP

Table 1 DSC and TGA data of EP and its composites

Samples	T_g (°C)	$T_{5\ wt\%}$ (°C)	$T_{50\ wt\%}$ (°C)	T_{max} (°C)	Residue at 700 °C (wt%)
EP	159.4	364.7	402.1	384.7	13.9
0.5GO/EP	160.3	368.2	368.2	385.7	15.2
0.5FR-fGO/EP	161.3	368.5	368.5	384.1	15.7
0.75FR-fGO/EP	161.5	366.2	366.2	384.1	15.8
1.0FR-fGO/EP	162.8	365.6	405.8	387.0	17.8

matrix and inhibited the decomposition of the polymer, which further retarded the release of combustible gases and caused a high decomposition temperature in the matrix.[31] When the amount of FR-fGO reached 1.0 wt% with the highest char residue of approximately 17.8%, FR-fGO exhibited the best thermal stability among all the samples. The DTG curves (Fig. S6b†) showed that the addition of FR-fGO significantly decreased the maximum mass loss rate (the peak of the DTG curves) of the EP composites, and the decomposed products would catalyze the charring of polymer chains and prevent mass loss during material combustion. The maximum thermal decomposition temperature shifted to a high temperature, especially when the amount of FR-fGO reached 1.0 wt% (387.0 °C) compared with pure EP (384.7 °C), which can be attributed to the fact that the flame-retardant FR-fGO and EP matrix formed a cross-linked network with good dispersion that improved the thermal stability of the EP composites.

3.3 Combustion properties

The combustion performances of EP and its EP composites were evaluated as follows. LOI and UL-94 tests are commonly used to evaluate the flammability of materials, and tests of all samples are summarized in Table 2. As shown in the table, the LOI value of pure EP was 26.4%. For the FR-fGO/EP samples, the LOI values were significantly increased. In addition, pure EP dripped easily after ignition. When small amounts of GO and FR-fGO were added, none of the EP samples had a classification in the UL-94 tests, showing that the amounts were insufficient to protect the EP matrix from decomposition. However, the dripping phenomenon of all samples disappeared during combustion. When the amount of FR-fGO reached 1.0 wt%, the fire became small until it was extinguished compared with other samples and reached a UL-94 V-1 rating. The aforementioned

Table 2 Flame-retardancy parameters obtained from the LOI and UL-94 tests

Samples	LOI (%)	Dripping	Ignition of cotton	UL-94
EP	26.4	Yes	Yes	No rating
0.5GO/EP	26.6	No	No	No rating
0.5FR-fGO/EP	26.8	No	No	No rating
0.75FR-fGO/EP	28.3	No	No	No rating
1.0FR-fGO/EP	29.2	No	No	V-1

results showed that the flame retardancy of EP can be effectively improved by the introduction of FR-fGO.

The influence of FR-fGO on the flame retardancy of EP was investigated using a cone calorimeter, which is an effective tool for evaluating the heat release of polymers, including heat release rate (HRR), total heat release (THR), smoke production rate (SPR), total smoke production (TSP), CO production rate, and CO_2 production rate. The relevant curves and data from the cone calorimetry tests are revealed in Fig. 5 and Table S1†. Pure EP burnt rapidly after ignition, with a sharp HRR (PHRR) of 1497.77 kW m^{-2} (Fig. 5a) and a high-peak SPR of 0.46 m^2 s^{-1} (Fig. 5c). At the end of combustion, the pure EP had lost >90% of its initial mass, with a THR of approximately 126.71 MJ m^{-2} (Fig. 5b), and total smoke yield of approximately 53.53 m^2 (Fig. 5d) because of its intrinsic and poor dispersion level and weak interfacial interactions with the EP matrix. Compared with pure EP, the introduction of 1 wt% FR-fGO reduced the PHRR from 1497.77 kW m^{-2} to 927.23 kW m^{-2}, and the THR also decreased by 41.4%. This phenomenon may be ascribed to the 1 wt% FR-fGO loading, which was generally used to give flame-retardant properties to the polymer due to its unique 2D sheet structure.[32] It is worth noting that there is only one HRR peak for the 1.0FR-fGO/EP composite, while pure EP has two peaks. The first peak is mainly due to the large amount of heat released by the combustion of the epoxy resin, while the second peak is due to the low strength of the char layer formed during the early combustion of the epoxy resin, which causes cracking and further combustion of the polymer matrix. In the combustion process, amino groups were introduced onto the GO surface, which were covalently incorporated into the EP matrix and improved the dispersion of nanosheets. In addition, due to the existence of ETEO, an Si-containing polymer cross-linked network formed in the EP matrix, which protected the matrix from further decomposition and inhibited the release of internal gases. The TSP, including CO_2 and CO, was reduced significantly, indicating a significant reduction in smoke toxicity. The physical barrier effect of the GO nanosheets can inhibit the escape of volatile decomposition products and flammable gases.[1] In addition, the residual mass of EP composites was higher than that of pure EP, which means that more EP matrix had been shielded from complete combustion. Thus, the fire safety of FR-fGO/EP composites is attributed to the good compatibility of functionalized graphene and the synergistic flame retardancy of FR-fGO.
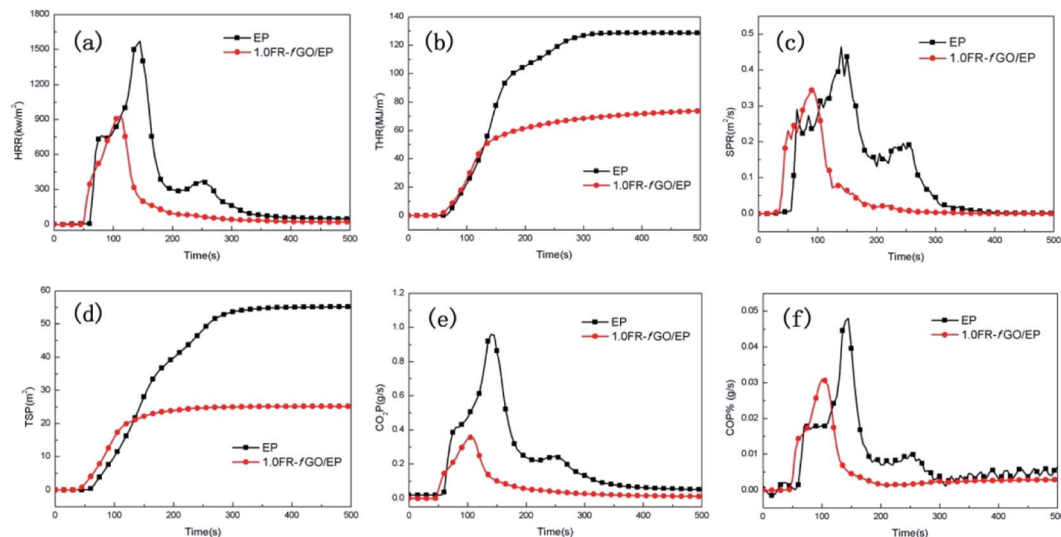
Fig. 5 HRR (a), THR (b), SPR (c), and TSP (d) *vs.* time curves of EP and its composites. CO (e) and CO_2 (f) yields *vs.* EP and its composites.

3.4 Char analysis

Photographs and the corresponding SEM images of EP-based composites after combustion in the cone calorimeter are presented in Fig. 6. After the combustion, a broken and fragile char residue was obtained for pure EP, and the internal matrix was finally burnt out (Fig. 6a). According to its SEM image (Fig. 6d), abundant cracks and holes were presented and could not efficiently protect the polymer matrix from combustion. When 0.5 wt% GO was incorporated into the EP matrix, a significant increase in char residue and few cracks and holes were observed in its SEM image (Fig. 6e). However, it still cannot effectively isolate the transfer of heat and O. Conversely, a compact and rigid char residue was formed in 1.0FR-fGO/EP, and no evident cracks were observed (Fig. 6f). The figure shows that the FR-fGO nanosheets were uniformly embedded in the EP matrix because FR-fGO sheets with amino groups on the surface were covalently bonded to the epoxy group. This result suggested that the internal released combustible gases and external heat can be inhibited from passing through during combustion.
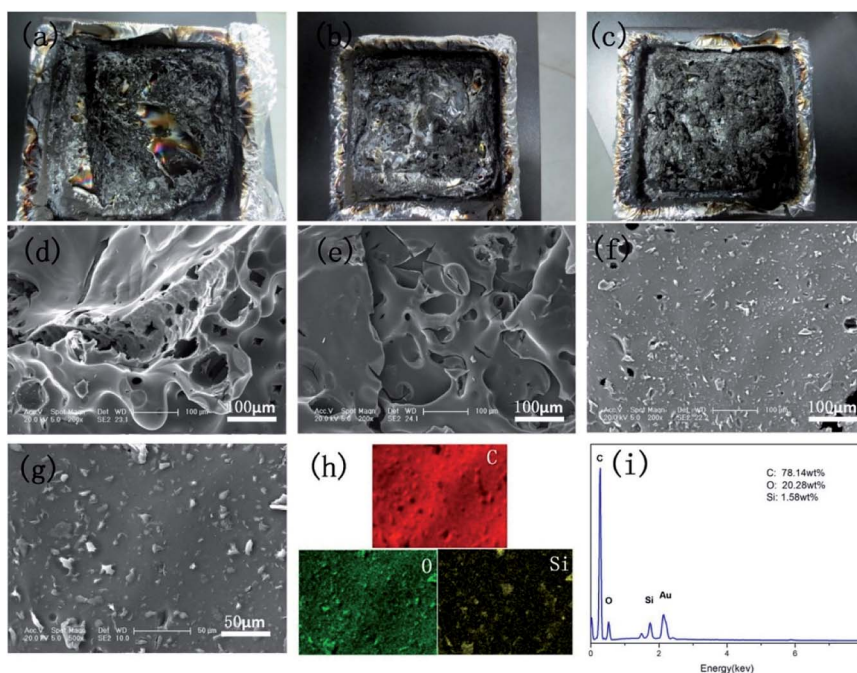

Fig. 6 Digital photographs of char residues after cone calorimeter tests: pure EP (a), 0.5GO/EP (b), and 1.0FR–fGO/EP (c) composites. SEM images of char structures obtained by cone calorimeter tests: pure EP (d), 0.5GO/EP (e), and 1.0FR–fGO/EP (f and g) composites. The element mapping (h) and EDX spectrum (i) of the 1.0FR–fGO/EP composite after calorimeter tests.

Meanwhile, the high-magnification SEM images (Fig. 6g) of the 1.0FR-fGO/EP composite and its EDX element mapping for the residues are illustrated in Fig. 6h and i. The results showed that a high Si concentration was detected, and Si-based char residues were formed due to the presence of an Si-containing cross-linked network. Meanwhile, a physical barrier effect and catalytic char residue, which can protect the internal matrix from further decomposition, were provided by graphene.

3.5 Gas phase analysis

Some studies have suggested that DDM has a good flame-retardant effect, which could generate non-combustible gases to form a gas barrier during combustion. However, this view had not been proved.[33,34] Here, a Py-GC/MS test was conducted to obtain the pyrolytic products of DDM. The gas chromatography spectra of DDM and its proposed pyrolysis process are shown in Fig. S7 and S8.† The main pyrolysis products of DDM were: phenol (b), phenol, 3-methyl- (c), benzenamine, 3-methyl-(d), p-cumenol (e), p-isopropenylphenol (f), and benzenamine, 4-(phenylmethyl)- (g). It was reported that nitrogenous compounds could be further decomposed to nitrogenous nonflammable gases, and dilute flammable gases and oxygen. During the decomposition process, we detected the presence of nitrogen, but the content was relatively low, indicating that the silicon–nitrogen-containing flame retardant works mainly in the solid phase. To study the decomposed volatiles of pure EP and its composites, we performed a TG-IR test from the thermal decomposition process at the maximum evolution rate. EP composites showed similar spectra to those of pure EP. And the characteristic peaks of the gaseous decomposition products, such as water (4000–3500 cm^{-1}), hydrocarbons (3200–2750 cm^{-1}), CO$_2$ (2358 and 2312 cm^{-1}), CO (2182 cm^{-1}), and aromatic compounds (1650–1410 cm^{-1}),[35–37] appeared, as shown in Fig. S9.† The total thermal degradation products of the 1.0FR-fGO/EP composite were similar to those observed for pure EP. However, the intensity of the gas release of the EP composite was significantly lower than that of pure EP (Fig. S9b†). The figure shows that the addition of 1.0FR-fGO significantly reduced the evolution of all gaseous organic volatiles, which was attributed to the enhancement in char formation and the physical barrier effect of the GO nanosheets. The well-dispersed FR-fGO nanosheets constituted a tortuous path, which prevented gas and heat exchange. Meanwhile, the decrement in organic pyrolysis volatiles effectively inhibits the release of smoke during combustion, because the condensed hydrocarbons and the aromatic compounds may be aggregated to form smoke[2]. Therefore, the addition of 1.0FR-fGO can efficiently reduce the fire hazards of the EP composite during combustion.

To confirm this point of view, we carried out Raman spectroscopy to determine the degree of graphitization of the char residues obtained from the cone calorimeter test, as shown in Fig. S10a and b.† The spectra of the two samples exhibited a similar shape with two peaks at 1590 and 1361 cm^{-1}, corresponding to D and G bands, respectively. The intensity ratio of the D and G bands (I_D/I_G) is often applied to estimate the degree

of graphitization of the residual char. Hence, the lower the I_D/I_G ratio, the higher the graphitization of the residual char.[38] The I_D/I_G ratio of pure EP was 1.77 (Fig. S10a†). But the 1.0FR-fGO/EP composite had a low I_D/I_G ratio of 1.12 (Fig. S10b†), indicating the formation of char with a high degree of graphitization and a thermally stable char structure. The incorporation of 1.0FR-fGO provided effective protection, reduced heat, and mass transfer between O and the matrix, which was in accordance with the TGA results. The increase in residual char was beneficial to the improvement in the thermal stability of EP. The XPS survey scans of the residual chars of pure EP and 1.0FR-fGO/EP composite are shown in Fig. S10c,† where can be seen the Si 2s and Si 2p peaks that appeared in the 1.0FR-fGO/EP composite. In addition, Fig. S8–10† displays the Si 2p spectra of the char layers of the 10FR-fGO/EP composite. There are two peaks at 101.5 and 102.1 eV, indicating that Si–C and Si–O bonds were formed in the char layers, further verifying the formation of the Si cross-linked network and participation in the charring process of composites during the combustion process.[38]

3.6 Flame-retardant mechanism of FR-fGO/EP composites

According to the discussion above, added FR-fGO can effectively enhance the fire-retardant properties of the EP composites. To explore the flame-retardant mechanism further, given that Si and N are the two of the most important halogen-free flame-retardant elements, the interaction energies of the Si–O and C–N bonds were investigated. The interaction energy of the Si–O bond had a value of −4.05 eV. However, the interaction energy of the C–N bond was −3.71 eV, which was higher than that of the Si–O bond that existed in FR-fGO. This result indicated that the C–N bond was preferentially decomposed compared with the Si–O bond in FR-fGO. As shown in Fig. 7, after ignition and heating, the FGO promoted char formation and the C–N bonds were broken first compared with Si–O bonds, according to the theoretical calculation. Thus, when the FR-fGO/EP composites were heated to a certain temperature, the N-containing groups on the GO sheet surface began to decompose and several holes and cracks appeared on the composite surface. In addition, some flammable gases (such as N$_2$) were released to reduce the flame intensity. Meanwhile, the FGO sheets gradually migrated to the surface of the substrate and acted as a physical barrier. With further thermal decomposition, the Si portion on GO began to decompose and formed an Si cross-linked network to the surface; this can prevent the further oxidation of residual chars, and formed stable residual chars and restricted the formation of holes and cracks. Thus, a compact and continuous char layer containing Si–O–Si was formed during combustion and participated in the charring process.

3.7 Mechanical properties

The elongation at break and tensile strength of EP and its various EP composites are observed in Fig. S11.† All EP composites had a longer elongation at break and a higher tensile strength than pure EP. The elongation at break of the 0.5FR-fGO/EP composite showed a pronounced improvement of
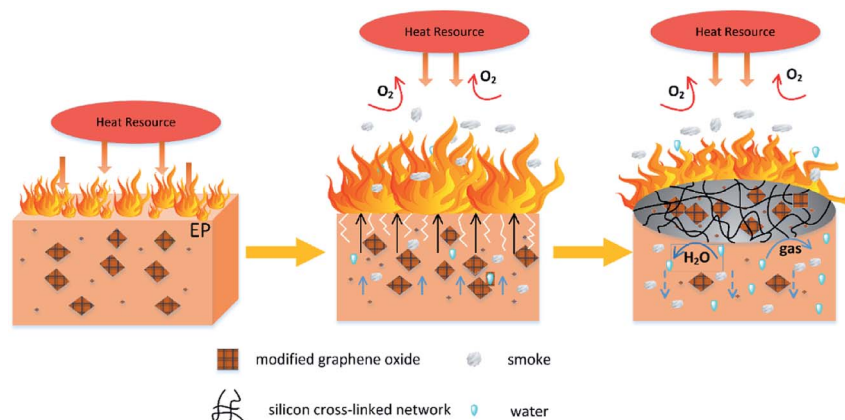
Fig. 7 Combustion process of FR–fGO/EP composites.

approximately 30%. The values of elongation at break showed an initial tendency to increase with loading of GO, I-GO, and FR-fGO, followed by a decrease after 0.5FR-fGO/EP. Generally, the elongation at break of the materials decreased as tensile strength increased. When the amount of added FR-fGO was >0.5 wt%, the higher the degree of cross-linked network formation, and the more brittle the materials, and the elongation at break decreased. The increased tensile strength up to 0.75FR-fGO showed good adhesion *via* a cross-linking chemical reaction between the –NH$_2$ groups in the FR-fGO molecules and the epoxy groups in the matrix. However, the decrease in the tensile strength of 1.0FR-fGO/EP could be an indication of the internal stress formed during EP curing, leading to poor mechanical performance.[39] Meanwhile, internal stress can be significantly decreased by incorporating soft segments (GO) into the EP matrix, which is more influential than the formation of a cross-linked network.[40–42] Therefore, the mechanical properties of the 1.0FR-fGO/EP composite are reduced.

3.8 Fracture surface of EP composites

Fig. 8 shows the fracture surface morphology of epoxy-based composites to understand the dispersion and interfacial interaction of FR-fGO in the matrix. Low-magnification SEM images (Fig. 8a–f) clearly show that the pure EP sample (Fig. 8a) exhibited a smooth structure and a river-like pattern with consistent directions, revealing poor mechanical properties. The other samples exhibited a rough surface, which suggested that different degrees of plastic deformation occurred before the fracture. The 1.0FR-fGO/EP composite surface (Fig. 8f) showed the roughest surface and the most uniform pattern among all the samples. In high-magnification SEM images (Fig. 8g–l), pure EP revealed a single-phase system, and the 0.5GO/EP system (Fig. 8h) showed several holes (yellow circles) and considerable aggregation, suggesting that the graphene sheets had poor interfacial interaction with the EP matrix. The 0.5I-GO/EP system (Fig. 8i) also showed slight agglomeration (red circles) on the graphene sheets. With further modification, several holes still appeared in the 0.5FR-fGO/EP system, but the distribution of nanosheets became uniform in the matrix (Fig. 8j). This finding may be attributed to the inability of the low FR-fGO content to form a homogeneous network in the matrix. Under the influence of external forces, a point defect was gradually enlarged at the two-phase interface, and the material was subsequently broken. Partly opened and unopened rough holes were observed as the amount of FR-fGO increased (Fig. 8k), suggesting the gradual formation of a polymer cross-linked network. When the amount of FR-fGO was approximately 1.0 wt% (Fig. 8l), the graphene network was formed, resulting in a rock-like fracture morphology without evident holes, and graphene was uniformly distributed in the matrix (red arrows). This result may be caused by the amino
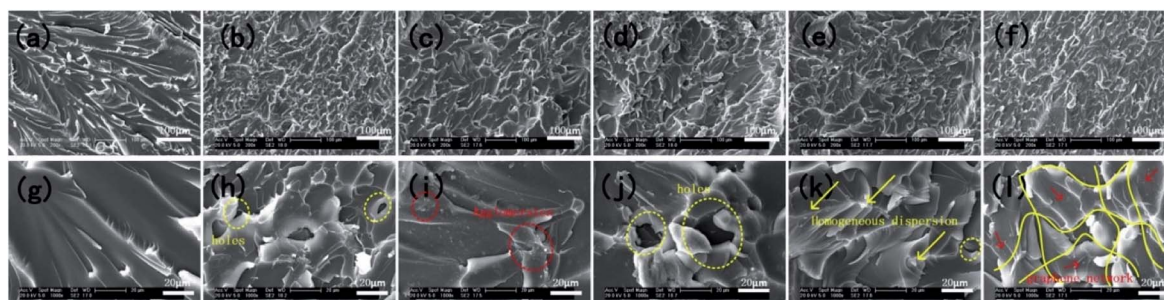

Fig. 8 SEM images of (a and g) pure EP, (b and h) 0.5GO/EP, (c and i) 0.5I–GO/EP, (d and j) 0.5FR–fGO/EP, (e and k) 0.75FR–fGO/EP, and (f and l) 1.0FR–fGO/EP composites.

group in the FR-fGO, which can readily react with the epoxy group in the EP matrix. The use of this amino group is beneficial in the formation of a cross-linked network and has the ability to cure EP to a certain degree. The network can increase char yield and restrain combustion. Its excellent mechanical properties can also effectively improve service life.[43]

4. Conclusions

An efficient and facile method was demonstrated to prepare a novel Si–N flame-retardant-wrapped GO for enhancement of the fire resistance and mechanical properties of EP. The flame retardant wrapped with active amine groups on the GO surface exhibited increased compatibility with the EP matrix through covalent bonding. The structure and morphology of FR-fGO were characterized well by FTIR, XRD, SEM, and TEM. The results showed that GO was successfully modified by an Si–N synergistic flame retardant. The obtained theoretical results were also consistent with the TGA results for FR-fGO. With the incorporation of FR-fGO into EP, a significant improvement in thermal stability in N_2 atmosphere, a maximum of 27 wt% improvement in char residues, and a 3.4 °C increase in the T_g of EP composites were observed. These results were attributed to the formation of an Si cross-linked network, which limited the movement of the matrix molecular chain. The flame retardancy of the EP composites also improved after the introduction of FR-fGO, and PHRR and THR were significantly reduced by 38.1% and 41.4%, respectively. The incorporation of FR-fGO also restrained the release of flammable volatiles, such as hydrocarbons and aromatic compounds. The significant improvements in the fire safety and smoke suppression of EP composites were considered to be a result of the barrier function of graphene, which was conducive to the formation of high char during combustion. Meanwhile, the elongation at break and tensile strength of the EP composites were also enhanced because of the remarkable dispersion in the matrix. This study provided a new direction in reducing the fire hazards of EP composites.

Conflicts of interest

The authors declare no conflict of interest.

Acknowledgements

References

1 S. Wang, R. Gao and K. Zhou, *J. Colloid Interface Sci.*, 2019, **536**, 127–134.

2 W. Cai, X. Feng, B. Wang, W. Hu, B. Yuan, N. Hong and Y. Hu, *Chem. Eng. J.*, 2017, **316**, 514–524.

3 Z. Sekhavat Pour and M. Ghaemy, *Compos. Sci. Technol.*, 2016, **136**, 145–157.

4 X. Wang, W. Xing, P. Zhang, L. Song, H. Yang and Y. Hu, *Compos. Sci. Technol.*, 2012, **72**, 737–743.

5 W. Cai, J. Wang, Y. Pan, W. Guo, X. Mu, X. Feng, B. Yuan, X. Wang and Y. Hu, *J. Hazard. Mater.*, 2018, **352**, 57–69.

6 Y. Li, D. Pan, S. Chen, Q. Wang, G. Pan and T. Wang, *Mater. Des.*, 2013, **47**, 850–856.

7 G. Yuan, B. Yang, Y. Chen and Y. Jia, *Composites, Part A*, 2019, **117**, 345–356.

8 G. Huang, S. Chen, S. Tang and J. Gao, *Mater. Chem. Phys.*, 2012, **135**, 938–947.

9 H. L. Ma, H. Bin Zhang, Q. H. Hu, W. J. Li, Z. G. Jiang, Z. Z. Yu and A. Dasari, *ACS Appl. Mater. Interfaces*, 2012, **4**, 1948–1953.

10 F. L. Jin, X. Li and S. J. Park, *J. Ind. Eng. Chem.*, 2015, **29**, 1–11.

11 R. Jian, P. Wang, W. Duan, J. Wang, X. Zheng and J. Weng, *Ind. Eng. Chem. Res.*, 2016, **55**, 11520–11527.

12 P. Wang and Z. Cai, *Polym. Degrad. Stab.*, 2017, **137**, 138–150.

13 Y. Han, T. Wang, X. Gao, T. Li and Q. Zhang, *Composites, Part A*, 2016, **84**, 336–343.

14 Y. Zhang, J. He and R. Yang, *Polym. Degrad. Stab.*, 2016, **125**, 140–147.

15 H. Yang, Y. Jiang, H. Liu, D. Xie, C. Wan, H. Pan and S. Jiang, *J. Colloid Interface Sci.*, 2018, **530**, 163–170.

16 M. Hajibeygi, M. Shabanian, H. Moghanian, H. A. Khonakdar and L. Häußler, *RSC Adv.*, 2015, **5**, 53726–53735.

17 T. Wu, J. Qiu, X. Lai, H. Li and X. Zeng, *Polym. Degrad. Stab.*, 2019, **159**, 163–173.

18 L. Qu, C. Zhang, P. Li, X. Dai, T. Xu, Y. Sui, J. Gu and Y. Dou, *RSC Adv.*, 2018, **8**, 29816–29829.

19 Z. Zhang, L. Yuan, Q. Guan, G. Liang and A. Gu, *Composites, Part A*, 2017, **98**, 174–183.

20 B. Yuan, Y. Sun, X. Chen, Y. Shi, H. Dai and S. He, *Composites, Part A*, 2018, **109**, 345–354.

21 R. Wang, D. Zhuo, Z. Weng, L. Wu, X. Cheng, Y. Zhou, J. Wang and B. Xuan, *J. Mater. Chem. A*, 2015, **3**, 9826–9836.

22 M. N. Li, Z. H. Zhang, S. Y. Wu and X. H. Chen, *Optik*, 2017, **148**, 344–349.

23 S. K. Mudedla, K. Balamurugan, M. Kamaraj and V. Subramanian, *Phys. Chem. Chem. Phys.*, 2016, **18**, 295–309.

24 J. I. Paredes, S. Villar-Rodil, A. Martínez-Alonso and J. M. D. Tascón, *Langmuir*, 2008, **24**, 10560–10564.

25 H. Yang, F. Li, C. Shan, D. Han, Q. Zhang, L. Niu and A. Ivaska, *J. Mater. Chem.*, 2009, **19**, 4632–4638.

26 B. Yu, Y. Shi, B. Yuan, S. Qiu, W. Xing, W. Hu, L. Song, S. Lo and Y. Hu, *J. Mater. Chem. A*, 2015, **3**, 8034–8044.

27 W. Yang, Y. R. Zhang, A. C. Y. Yuen, T. B. Y. Chen, M. C. Chan, L. Z. Peng, W. J. Yang, S. E. Zhu, B. H. Yang, K. H. Hu, G. H. Yeoh and H. D. Lu, *Chem. Eng. J.*, 2017, **321**, 257–267.

28 Y. Feng, C. He, Y. Wen, Y. Ye, X. Zhou, X. Xie and Y. W. Mai, *Composites, Part A*, 2017, **103**, 74–83.

29 W. Hu, B. Yu, S. D. Jiang, L. Song, Y. Hu and B. Wang, *J. Hazard. Mater.*, 2015, **300**, 58–66.

30 M. Khajehzadeh and N. Sadeghi, *J. Mol. Liq.*, 2018, **256**, 238–246.

31 X. Wang, L. Song, W. Pornwannchai, Y. Hu and B. Kandola, *Composites, Part A*, 2013, **53**, 88–96.

32 K. Zhou, B. Wang, J. Liu, S. Jiang, Y. Shi, Q. Zhang, Y. Hu and Z. Gui, *Mater. Res. Bull.*, 2014, **53**, 272–279.

33 Y. Feng, J. Hu, Y. Xue, C. He, X. Zhou, X. Xie, Y. Ye and Y. W. Mai, *J. Mater. Chem. A*, 2017, **5**, 13544–13556.

34 H. Wang, H. Qiao, J. Guo, J. Sun, H. Li, S. Zhang and X. Gu, *Composites, Part B*, 2020, **182**, 107498.

35 J. Wang, J. Zhan, X. Mu, X. Jin, F. Chu, Y. Kan and W. Xing, *J. Colloid Interface Sci.*, 2018, **529**, 345–356.

36 Y. Feng, C. He, Y. Wen, Y. Ye, X. Zhou, X. Xie and Y. W. Mai, *J. Hazard. Mater.*, 2018, **346**, 140–151.

37 B. Yu, W. Xing, W. Guo, S. Qiu, X. Wang, S. Lo and Y. Hu, *J. Mater. Chem. A*, 2016, **4**, 7330–7340.

38 W. C. Wei, C. Deng, S. C. Huang, Y. X. Wei and Y. Z. Wang, *J. Mater. Chem. A*, 2018, **6**, 8643–8654.

39 Z. K. Chen, G. Yang, J. P. Yang, S. Y. Fu, L. Ye and Y. G. Huang, *Polymer*, 2009, **50**, 1316–1323.

40 H. Gu, C. Ma, J. Gu, J. Guo, X. Yan, J. Huang, Q. Zhang and Z. Guo, *J. Mater. Chem. C*, 2016, **4**, 5890–5906.

41 G. Yang, S. Y. Fu and J. P. Yang, *Polymer*, 2007, **48**, 302–310.

42 D. J. Liao, Q. K. Xu, R. W. McCabe, H. V. Babu, X. P. Hu, N. Pan, D. Y. Wang and T. R. Hull, *Ind. Eng. Chem. Res.*, 2017, **56**, 12630–12643.

43 H. Y. Ma, L. F. Tong, Z. Bin Xu and Z. P. Fang, *Adv. Funct. Mater.*, 2008, **18**, 414–421.